

Electric-field control of exchange interactionsS. Mankovsky¹, E. Simon¹, S. Polesya¹, A. Marmodoro², and H. Ebert¹¹*Department of Chemistry/Phys. Chemistry, LMU Munich, Butenandtstrasse 11, D-81377 Munich, Germany*²*Institute of Physics, Czech Academy of Sciences, Cukrovarnicka 10, 162 00 Praha 6, Czech Republic*

(Received 4 August 2021; revised 8 November 2021; accepted 15 November 2021; published 30 November 2021)

The impact of an applied electric field on exchange coupling parameters has been investigated based on first-principles electronic structure calculations by means of the Korringa-Kohn-Rostoker Green function method. The calculations have been performed for a Fe film, free-standing and deposited on two different substrates, having 1 monolayer (ML) thickness to minimize the effect of screening of the electric field typical for metallic systems. By comparing the results for the free-standing Fe ML with those for Fe on the various substrates, we could analyze the origin of the field-induced change of the exchange interactions. Compared to the free-standing Fe ML, in particular rather pronounced changes have been found for the Fe/Pt(111) system due to the localized electronic states at the Fe/Pt interface, which are strongly affected by the electric field and which play an important role for the Fe-Fe exchange interactions.

DOI: [10.1103/PhysRevB.104.174443](https://doi.org/10.1103/PhysRevB.104.174443)**I. INTRODUCTION**

The control of magnetic properties by applying an electric field has been discussed in the literature for many years [1–12]. Apart from the well-known example of magnetocrystalline anisotropy (MCA) influenced by an electric field [5,13–16], various types of magnetoelectric (ME) effects have been discussed. Accordingly, quite a large number of investigations have been devoted to antiferromagnetic (AFM) [9,17–19], noncollinear magnetic [1,20], or ferromagnetic (FM) [3,8,21–24] systems. In the case of FM materials, the investigations have focused in particular on the dependence of exchange interactions on an applied electric field, with the aim of manipulating the ferromagnetic-to-paramagnetic transition. The features of the ME effect depend in turn on the dominating exchange mechanism in the material [3]. In the diluted magnetic semiconductor (DMS) (In,Mn)As [21,22], for instance, used as a prototype system within such investigations, the dominating Ruderman-Kittel-Kasuya-Yosida (RKKY) exchange is mediated by holes, and it depends strongly on the hole concentration, which may be efficiently controlled by the applied electric field. In the case of metallic materials, the situation is more complicated [23] as their magnetic properties are governed by exchange interactions that have quite a different origin and consequently a different behavior under an applied electric field. It is worth noting in addition that despite a short screening length in metals [3], a rather pronounced magnetoelectric effect was demonstrated within density functional theory (DFT) calculations performed for thin metallic Fe(001), Ni(001), and Co(0001) films [8]. Experimentally, a significant field-induced change of the Curie temperature T_C was observed for Co ultrathin films embedded into different layered structures [6,25]. The dependence of T_C on the electric-field strength was attributed to the corresponding modification of the interatomic exchange interactions J_{ij} . As was mentioned above, the origin of these changes in

metallic films is different compared to DMS materials, and explicit first-principles calculations of the exchange coupling parameters would be very desirable to find out the relationship between the field-induced modification of J_{ij} and the electronic structure in the system, as has been done, for instance, for free-standing Fe(001) and Co/Pt(111) [26] FM films.

Because of the central role of the Dzyaloshinskii-Moriya interaction (DMI) in two-dimensional layered systems for the formation of magnetic skyrmions, control of the DMI by an applied electric field is of great interest as it enables us to manipulate the stability of skyrmions. In fact, a strong variation of the DMI with electric field was found experimentally for the Ta/FeCoB/TaO [27] and MgO/Fe/Pt [28] trilayer systems. The impact of the electric field on the size of the magnetic domain wall, investigated experimentally for Pt/Co [29] and Pt/Co/AlO_x [30] thin films, and its impact on the domain wall motion in Pt/Co/Pd films [31], were also associated with the field-induced change of the Dzyaloshinskii-Moriya interaction. Furthermore, there is also great interest in the ME effect in bulk noncollinear magnetic materials [1,20], which is also associated with the electric-field-induced DMI.

Despite significant attention devoted in the literature to the magnetoelectric effect, so far no systematic investigations have been performed on a first-principles level. To our knowledge, there are only a few corresponding reports in the literature, one of which is the above-mentioned report by Oba *et al.* [26] on the field-dependent J_{ij} for free-standing Fe(001) and Co/Pt(111). Yang *et al.* [32] have studied the electric-field control of the DMI for the NM/Co/Pt trilayers with different nonmagnetic NM layers. Recently, Paul and Heinze [33] reported on the stability of skyrmions controlled by the electric field, where J_{ij} , \vec{D}_{ij} , biquadratic interactions, and MCA have been calculated on the same footing on an *ab initio* level.

In this work, we focus on three prototype systems: the free-standing Fe monolayer (ML), 1 ML Fe deposited on Pt(111), and 1 ML Fe deposited on 1H-WS₂ substrates. The first-principles calculations of the electronic structure and the exchange interactions and DMI for these systems have been performed without an external electric field as well as in the presence of the electric field to reveal the relation between the field-induced changes of the electronic structure and the exchange parameters.

II. COMPUTATIONAL DETAILS

Within the present work, exchange coupling parameters were calculated using the spin-polarized relativistic-Korringa-Kohn-Rostoker (SPR-KKR) Green function method [34,35]. The fully relativistic mode was used throughout except for those cases for which a scaling of the spin-orbit interaction was applied. All calculations have been performed within the framework of the local spin density approximation (LSDA) to spin density functional theory (SDFT), using the parametrization for the exchange and correlation potential as given by Vosko *et al.* [36]. The charge and spin densities as well as the potentials were treated on the level of the atomic sphere approximation (ASA). A cutoff $l_{\max} = 3$ was used for the angular momentum expansion of the Green function. The k -space integration over the two-dimensional (2D) Brillouin zone (BZ) was done using a 109×109 2D k -mesh.

The calculations for 1 ML of Fe deposited on the Pt(111) surface have been performed for a geometry consisting of semi-infinite Pt and vacuum subspaces to the left and to the right, respectively, of the so-called interaction zone consisting of three atomic layers of Pt, one layer of Fe, and five layers of empty spheres (vacuum). The calculations for a free-standing Fe monolayer and 1 ML Fe on WS₂ have been performed in slab geometry. In the latter case, there are two possibilities for the arrangement of the Fe atoms with respect to the position of W in 1H-WS₂, i.e., being either above the W atoms or above vacancies within the W layer. As the former occupation is energetically more preferable, all calculations here have been done for Fe occupying positions above the W atoms, with identical Fe-S and W-S distances. Finally, it should be noted that for all calculations the structure relaxation of the surface layers has not been taken into account.

Within the present work, we investigate the impact of an electric field on the magnetic properties of metallic FM films restricting to the situation when the field is applied along the normal to the surface. This implies that the electric field will lead to some charge rearrangement but not to a steady-state electric current. We focus here on ultrathin films considering one Fe monolayer, as in this case one can expect pronounced effects while these will be reduced in metallic bulk materials because of screening (see, e.g., Ref. [37]). Accordingly, we consider here as representative examples a 1ML Fe film deposited on different substrates. To clarify the role of the substrate, we represent also results for an unsupported Fe monolayer.

Dealing with an Fe monolayer, one has to make a comment concerning its magnetic ordering. It is well known that the magnetic order in an ideal 2D system should be broken at $T > 0$ K due to spin-wave (SW) excitations, as is to be expected on

the basis of the Mermin-Wagner theorem [38]. This, however, does not hold in the presence of magnetic anisotropy, which causes for the SW spectrum the opening of an energy gap at the $\bar{\Gamma}$ point of the 2D BZ and thus blocks the low-energy SW excitations [39]. As a consequence, this mechanism leads to a dependence of the Curie temperature, T_C , on the MCA [40]. Accordingly, one may expect a possible impact of the electric field on T_C due to the field-dependent changes of the MCA discussed in the literature.

In the present work, we assume a finite MCA to ensure a unique FM order in the Fe film. However, we do not discuss the impact of the electric field on the MCA and on the Curie temperature. Instead, we focus on the behavior of the exchange parameters J_{ij} and \vec{D}_{ij} that represent the isotropic and anisotropic Dzyaloshinskii-Moriya interaction, respectively. Their field dependence will be monitored using the Curie temperature T_C^{MFA} evaluated via mean-field theory.

For the electronic structure calculations, the effect of a homogeneous external electric field was modeled by a periodic array of point charges in the vacuum region that behave essentially like a charged capacitor plate. This leads to a homogeneous electric field of strength

$$E = \frac{Q}{2A\epsilon_0}, \quad (1)$$

where Q is the charge of the capacitor in units of the electron's charge, ϵ_0 is the permittivity of vacuum, and A is the area per charged site in the capacitor plate. As suggested by Eq. (1), the orientation of the electric field can be controlled via the sign of Q . A positive charge Q in front of a surface gives rise to a field $\vec{E} = E_z \hat{z}$ pointing inwards to the bulk and antiparallel to the surface normal \hat{z} . As E_z in this case, the electric field will be denoted briefly "negative," while "positive" denotes an outward-oriented electric field.

III. RESULTS

A. Free-standing 1 ML Fe

Presenting our results, we start with the free-standing Fe monolayer having a hexagonal structure with its structure parameters corresponding to 1 ML Fe deposited on a Pt(111) surface ($a_{\text{lat}} = 5.24$ a.u.). The spin magnetic moment of Fe calculated for this 2D system is $3.013\mu_B$. Considering a monolayer film, the system experiences accordingly the influence of the electric field without screening. As was discussed by Nakamura *et al.* [13] and Oba *et al.* [26], the external electric field $\vec{E} = E_z \hat{z}$ along the film normal \hat{z} introduces a perturbation to the system according to the Hamiltonian $\mathcal{H}^{(1)} = -\sqrt{\frac{4\pi}{3}} eE_z Y_{1,0}$ creating a coupling of the l - and $(l \pm 1)$ -type orbitals with equal magnetic quantum number m , i.e., for examples d_{z^2} and p_z as well as d_{xz} , d_{yz} and p_x , p_y orbitals. This can be seen in the Bloch spectral function (BSF) plotted in Fig. 1(a), right panel, in comparison with the BSF for the nondistorted system shown in the left panel as a reference. In the former case, the avoided crossings can be seen for the energy bands in the middle of the $\bar{\Gamma}$ - \bar{M} and $\bar{\Gamma}$ - \bar{K} directions, being a consequence of such a p - d hybridization. The change in the charge density $\rho^{(1)} \sim -\frac{1}{\pi} \text{Im Tr} \int d\mathcal{E} Y_{1,0} G(\mathcal{E}) \mathcal{H}^{(1)} G(\mathcal{E})$ arising as a response to the external electric field creates in

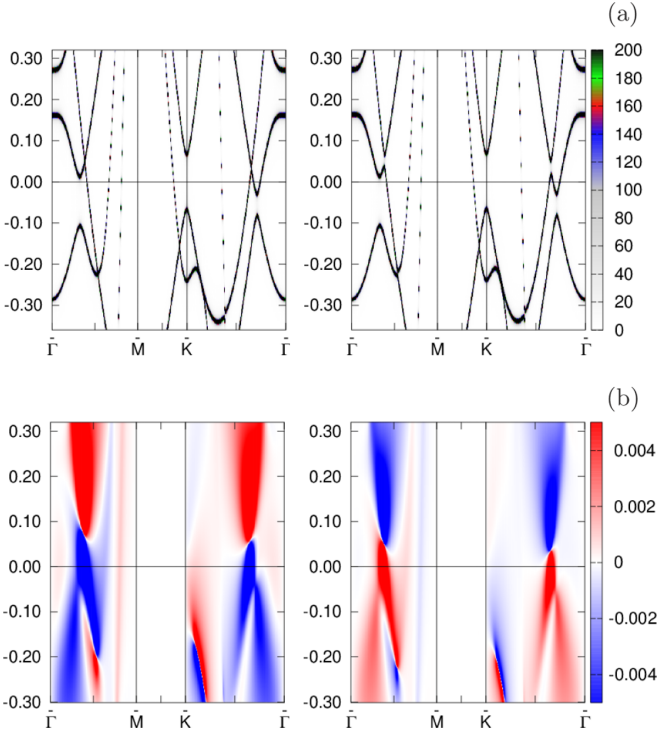


FIG. 1. (a) Calculated Bloch spectral function $A(\mathcal{E}, \vec{k}, 0)$ (left panel) and $A(\mathcal{E}, \vec{k}, E)$ with $E = 13.6 \frac{\text{V}}{\text{nm}}$ (right panel) for the unsupported Fe monolayer. (b) Spin polarization along the \hat{x} direction of the electronic states in the presence of an electric field $E = -13.6 \frac{\text{V}}{\text{nm}}$ (left) and $E = 13.6 \frac{\text{V}}{\text{nm}}$ (right),

turn an induced electric polarization breaking the inversion symmetry of the film.

As follows from the calculations, the Fe spin magnetic moment is practically unchanged by the applied electric field. Nevertheless, there is a noteworthy change for the exchange coupling parameters, which are shown up to the third atomic shells in Fig. 2 (left panel) as a function of the electric-field strength. As one can see, the weak modification of J_{ij} due to the electric field has an almost parabolic dependency. It can be ascribed to the shift of the Fermi level and to the change of hybridization of the localized d and delocalized p electrons mediating interatomic exchange interactions. Considering the electric field as a perturbation, one can expand the exchange coupling parameter in powers of the electric field. This expansion has contributions only from even powers with respect to \vec{E} to ensure a scalar character for J_{ij} . This leads to a parabola-like dependence of this quantity on the electric field. As will be shown below, the field-dependent variation of J_{ij} parameters corresponding to deposited Fe monolayers is more complicated due to other field-induced effects having an impact on the exchange interactions.

The broken inversion symmetry due to the presence of an external electric field \vec{E} creates a nonzero DMI, which is shown in the right panel of Fig. 2. As one can see, the DMI increases linearly with the field strength and accordingly changes sign when the field changes its direction. This behavior is associated with the field-induced Rashba SOC that introduces a perturbation to the delocalized electrons

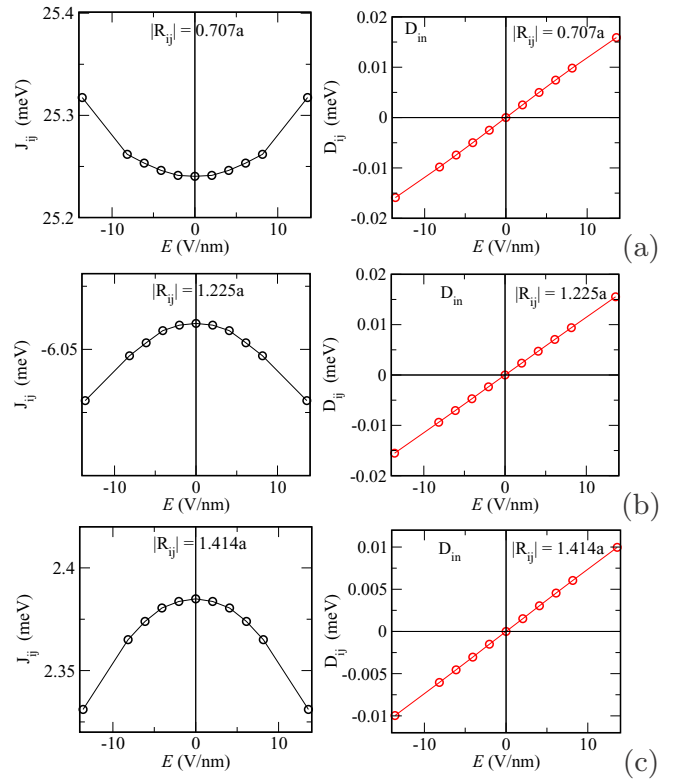


FIG. 2. Isotropic Fe-Fe exchange coupling parameter \bar{J}_{ij} (left panel) and the maximal in-plane component of DMI, \bar{D}_{ij}^{in} , characterizing the interactions with the first-neighbor at $R_{01} = 0.707a$ (a), second-neighbor at $R_{02} = 1.225a$ (b), and third-neighbor at $R_{03} = 1.414a$ (c), for a free-standing Fe monolayer.

mediating the Fe-Fe exchange interaction according to the expression [41]

$$\mathcal{H}_R = \frac{\alpha_R}{\hbar} (\hat{z} \times \vec{p}) \cdot \vec{\sigma}, \quad (2)$$

with the Rashba parameter $\alpha_R \sim E_{\text{eff}}$, where the effective electric field E_{eff} is created by the external and induced, $E_{\text{ind}} = -\nabla_z \delta\phi[\rho^{(1)}]$, electric fields (where $\delta\phi[\rho^{(1)}]$ is the field-induced potential). To demonstrate the impact of the Rashba-type SOC on the electronic structure, we plot in Fig. 1(b) the in-plane spin polarization (\hat{x} -projection) of the electronic states, which does not show up in the field-free system as well as in the case of SOC strength artificially scaled down to zero. Moreover, this spin polarization having different directions for different energy bands changes sign to the opposite together with the electric-field direction (similar behavior to that observed for the DMI), which can be seen by comparing the left and right panels in Fig. 1(b). To have a more complete picture, Fig. 3(a) shows the calculated Bloch spectral functions $A(\mathcal{E}_F, \vec{k}_{\parallel}, E)$ (left panel) and $A(\mathcal{E}_F + \delta, \vec{k}_{\parallel}, E)$ (right panel), with $\delta = 0.2 \text{ eV}$ and $E = 13.6 \frac{\text{V}}{\text{nm}}$, representing the cut of the energy bands by the energy planes $\mathcal{E} = \mathcal{E}_F$ and $\mathcal{E} = \mathcal{E}_F + 0.2 \text{ eV}$. The corresponding \hat{x} -projected spin polarization for these energy bands is displayed in Fig. 3(b). It has a different sign for the states with $\mathcal{E} = \mathcal{E}_F$ and $\mathcal{E} = \mathcal{E}_F + 0.2 \text{ eV}$, located around the $\bar{\Gamma}$ point. Taking into account also the \hat{y} -projected spin polarization, one can reproduce the

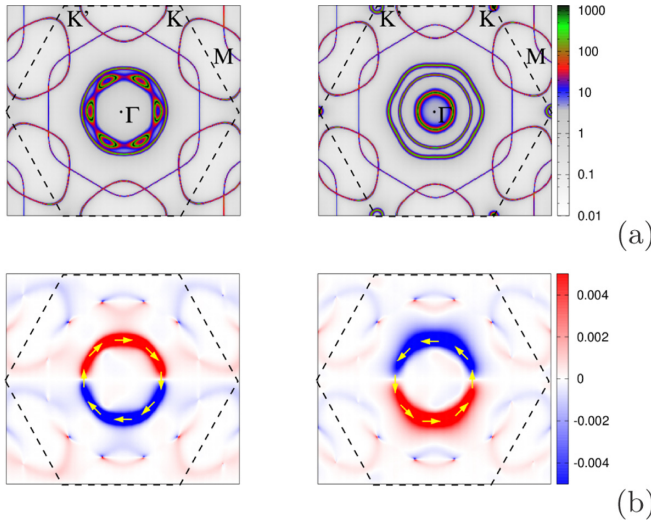


FIG. 3. (a) Calculated Bloch spectral function $A(\mathcal{E}_F, \vec{k}_{\parallel}, E)$ (left panel) and $A(\mathcal{E}_F + \delta, \vec{k}_{\parallel}, E)$ (right panel) with $\delta = 0.2$ eV and $E = 13.6 \frac{\text{V}}{\text{nm}}$, for the unsupported Fe monolayer, and (b) corresponding \hat{x} -spin polarization of these electronic states.

orientation of the in-plane spin polarization shown in Fig. 3(b) by yellow arrows. It is worth noting the Rashba SOC-induced modification of the electronic structure seen in Fig. 3(a), right panel, with small electronic pockets in the \bar{K} and \bar{K}' symmetric points of 2D BZ having a different size in the presence of the electric field, but becoming identical in the case of SOC switched off.

The DMI caused by the Rashba SOC was discussed already in the literature, e.g., by Kundu and Zhang [42]. For this reason, we only point out that in the particular case of a free-standing Fe monolayer, all three DMI parameters presented in Fig. 8 (right panel) have the same order of magnitude. Positive orientations of the DMI vectors are shown in Fig. 4.

B. 1 ML Fe/Pt(111)

Next, we consider a 1 ML Fe film on a Pt(111) substrate. The change of the spin magnetic moment in the Fe monolayer, m_{Fe} , due to an applied electric field is shown in Fig. 5. The most significant change occurs at a small strength of the electric field, with an almost linear dependence of $m_{\text{Fe}}(E)$ on the electric-field strength. With further increasing field strength, $|\vec{E}| > 5 \frac{\text{V}}{\text{nm}}$, the magnetic moment shows only a weak

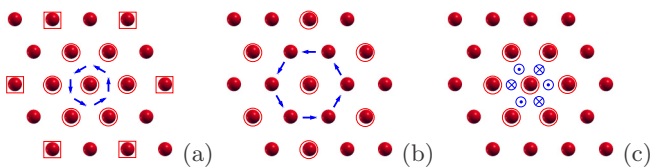


FIG. 4. The structure of the Fe monolayer and the positions of first- [(a), shown by cycles], second- (b), and third-neighbor [(a), shown by squares] atoms. Positive directions of the in-plane components of DMI, \vec{D}^{in} , are shown by blue arrows. Part (c) represents the out-of-plane DMI component, \vec{D}^{out} , alternatively changing sign coming from atom to atom within the atomic shell.

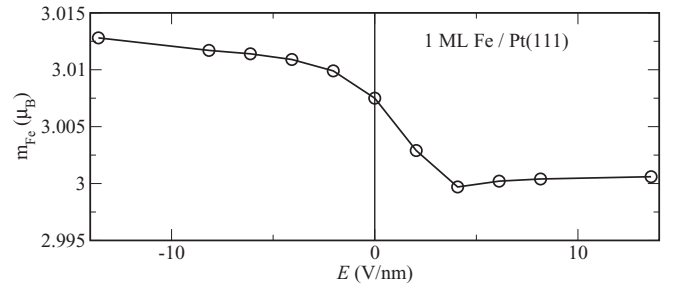


FIG. 5. Calculated spin magnetic moment of Fe, $m_{\text{Fe}}(E)$, as a function of the external electric field E for 1 ML Fe on Pt(111).

variation with the field. To demonstrate the impact of the electric field on the electronic structure, we plot in Fig. 6 the difference in the Bloch spectral function $A(\mathcal{E}, \vec{k}, E) - A(\mathcal{E}, \vec{k}, 0)$, representing the changes of the (a) Fe- and (b) Pt(I)-projected electronic states due to a negative ($E = -13.6 \frac{\text{V}}{\text{nm}}$; left) and positive ($E = 13.6 \frac{\text{V}}{\text{nm}}$; right) electric field, with Pt(I) denoting the Pt atoms at the Fe/Pt interface. As one can see, the Fe layer experiences the strongest influence of the electric field. The modification of the band structure due to the electric field for 1 ML Fe on Pt(111) is obviously more complex than for the free-standing Fe

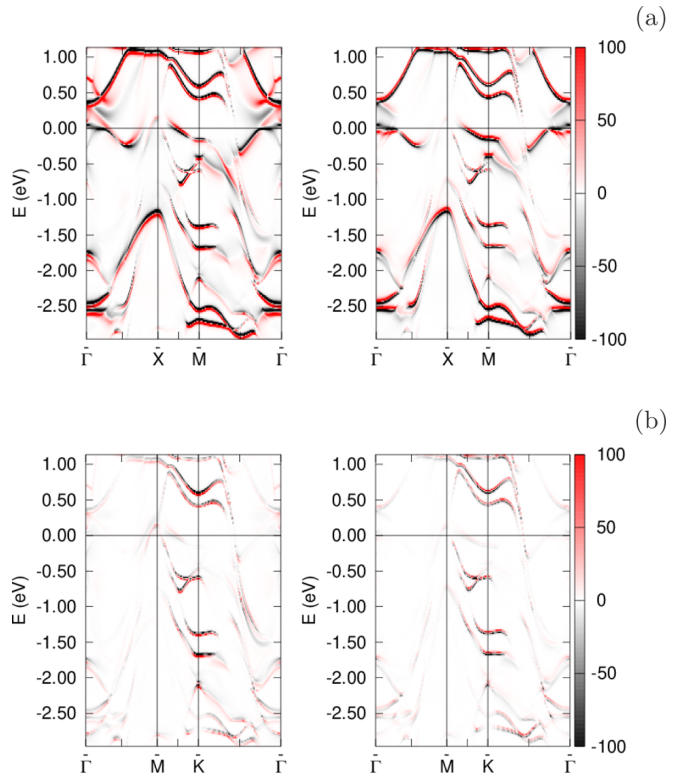


FIG. 6. Calculated difference in the Bloch spectral function $A(\mathcal{E}, \vec{k}, E) - A(\mathcal{E}, \vec{k}, 0)$, demonstrating the field-induced changes of the Fe- (a) and Pt(I)-projected (b) electronic states [Pt(I) denotes the Pt layer at the Fe/Pt interface] in 1 ML Fe on Pt(111). Red and black colors correspond to the modified and nonmodified states, respectively, in the presence of negative, $E = -13.6 \frac{\text{V}}{\text{nm}}$ (left), and positive, $E = +13.6 \frac{\text{V}}{\text{nm}}$ (right).

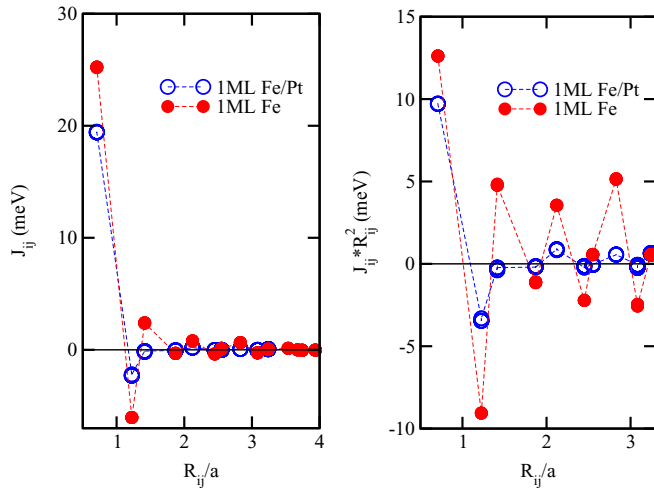


FIG. 7. Isotropic Fe-Fe exchange coupling parameter J_{ij} as a function of the interatomic distance R_{ij} for a nondistorted 1 ML Fe on Pt(111) (open symbols) and for a free-standing Fe monolayer (full symbols) (left panel). The right panel represents the product $J_{ij}R_{ij}^2$ as a function of the squared distance R_{ij}^2 .

monolayer. As was already discussed previously [37], one can distinguish several mechanisms for the observed field-induced changes in the electronic structure. First of all, one notes a shift of the electronic states, which depends on their distance to the surface. This shift is the strongest for the states well localized in the surface region with an unscreened or weakly screened electric field. In Fig. 6(a), one can see in particular a pronounced field-induced shift for the Fe d -states, while the shift for the Pt states at the Pt/Fe interface is weaker. This is a result of a partial screening of the electric field as well as a weaker localization of the electron Pt states.

As was pointed out above, the applied electric field changes in addition the hybridization [26] of the p - and d - states. This effect, however, is hard to see in Fig. 6 because of the strong modification of the electronic states of deposited Fe when compared to a single Fe monolayer.

Finally, one notes that the bulklike Pt states are almost unmodified. As a result, the field-induced shifts of the Fe d -states having essentially 2D character are accompanied by a corresponding broadening, as is seen in Fig. 6, which is a consequence of their modified hybridization with the bulklike Pt energy bands.

Concerning the field dependence of the isotropic exchange coupling parameters, Fig. 7 shows these as a function of interatomic distance R_{ij} for the field-free case as a reference (left panel, open symbols). As can be concluded from the oscillating behavior of the product $J_{ij}R_{ij}^2$ given in the right panel in Fig. 7, they show a well-defined RKKY-like characteristic for large distances. These interactions are compared with those calculated for the free-standing Fe monolayer, shown by full symbols. For all distances, the Fe-Fe interactions are stronger for the free-standing Fe monolayer, a finding that can be associated with a narrower d -band and higher DOS at the Fermi energy, leading to a larger energy change under the perturbation caused by spin tiltings. Although the oscillations in both cases have a different amplitude, the parameter J_{ij}

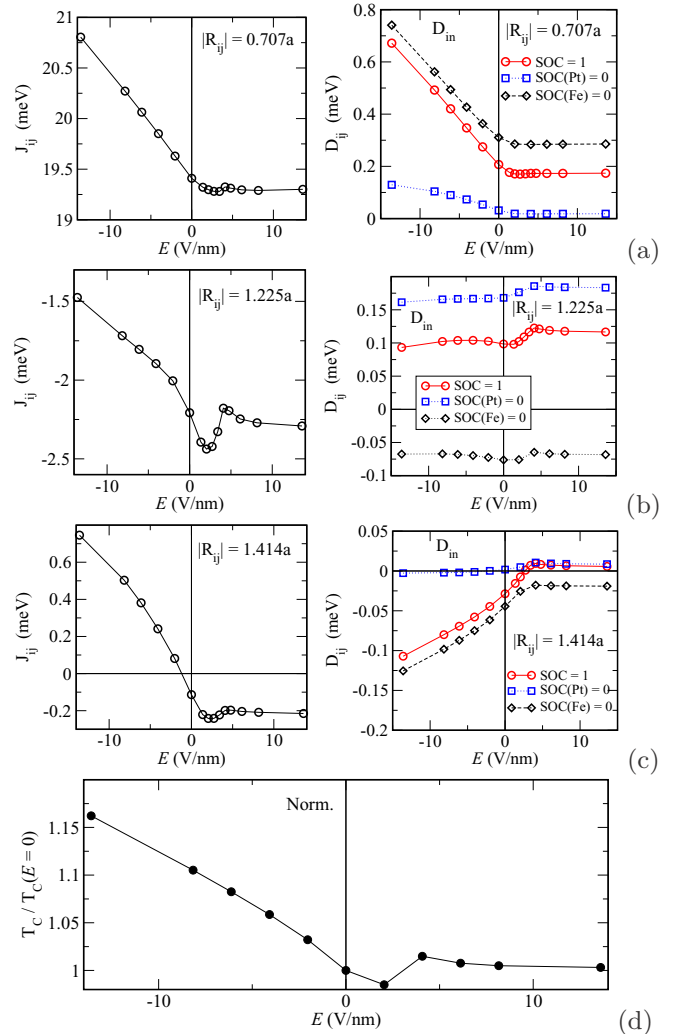


FIG. 8. Isotropic Fe-Fe exchange-coupling parameter J_{ij} (left panel) and the maximal in-plane components of DMI, \vec{D}_{ij}^{in} (right panel), characterizing the interaction with the first neighbors at $R_{01} = 0.707a$ (a), the second neighbors at $R_{02} = 1.225a$ (b), and the third neighbors at $R_{03} = 1.414a$ (c), for 1 ML Fe on Pt(111). The parameters are plotted as a function of the applied electric field. (d) Reduced Curie temperature $T_C/T_C(E=0)$ as a function of the electric field, with $T_C(E=0) = 801$ K, determined on the basis of mean-field theory.

has a similar RKKY-like dependency on the distance R_{ij} . Figure 8 (left panel) represents the exchange-coupling parameters J_{01} (for $R_{01} = 0.707a$), J_{02} (for $R_{02} = 1.225a$), and J_{03} (for $R_{03} = 1.414a$) as a function of the electric field. As one can see, the relative change of the first-neighbor parameter J_{01} is rather small, while the change is more pronounced for the two other parameters that are negative in sign for the field-free case. However, both parameters, J_{02} and J_{03} , are substantially smaller when compared to J_{01} , implying that they play a much weaker role for the magnetic properties of the system, which is expected to be ferromagnetic (FM) due to dominating FM interactions J_{01} . As one can see in Fig. 8, all parameters increase almost linearly together with increasing “negative” electric field, leading for J_{03} to a change in sign. An increasing “positive” field, on the other hand, leads to a saturation already

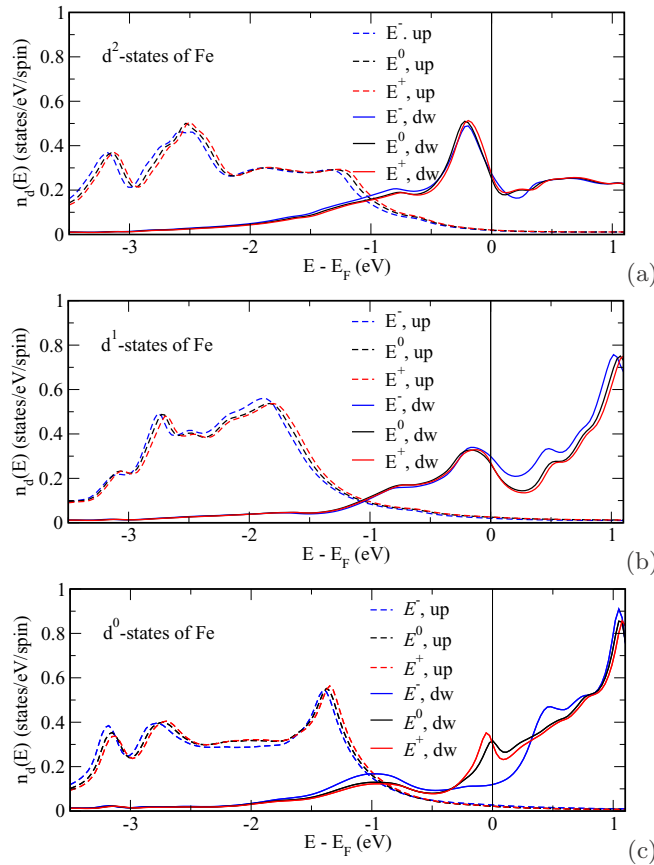


FIG. 9. Electric-field-induced change of the (l, m, s) resolved density of states in the Fe layer on Pt(111). The applied electric field $E^0 = 0.0$ V/nm, $E^+ = +13.6$ V/nm, and $E^- = -13.6$ V/nm.

at $E > 5 \frac{\text{V}}{\text{nm}}$. To get an impression for the influence of the electric field on the Curie temperature T_C , we plot in Fig. 8(d) $T_C^{\text{MFA}}(|\vec{E}|)$ calculated using the exchange coupling parameters in Figs. 8(a)–8(c) on the basis of the mean-field theory. Obviously, $T_C^{\text{MFA}}(|\vec{E}|)$ follows the field-induced changes of J_{ij} shown in Figs. 8(a)–8(c), exhibiting a strong field dependence for “negative” field and only weak changes for “positive” fields.

As one can see in Fig. 6, a “positive” electric field leads in general to an upward shift for the d -states of Fe, while a “negative” field leads to a shift of the states down in energy. The same trend can be seen for the (l, m, s) -resolved DOS plotted in Figs. 9(a) and 9(b) showing the DOS for the $d_{x^2-y^2}$, d_{xy} , d_{xz} , and d_{yz} states. However, pronounced field-induced shifts of the electronic states occur around the Γ point in the vicinity of the Fermi energy for a “negative” field. This shift is opposite in direction compared to all others. As is shown in Fig. 9(c), a strong modification of the minority-spin d_{z^2} states occurs close to the Fermi energy for a “negative” field. This shift is also seen in Fig. 10 giving the BSF for the minority-spin states of Fe. As one can see, the states at the Γ point move in the presence of an electric field from a position close to the Fermi level upward in energy into the energy gap of the bulk Pt states. These states have to be seen as interface states strongly affected by the weakly screened electric field due to their spatial position. On the other hand,

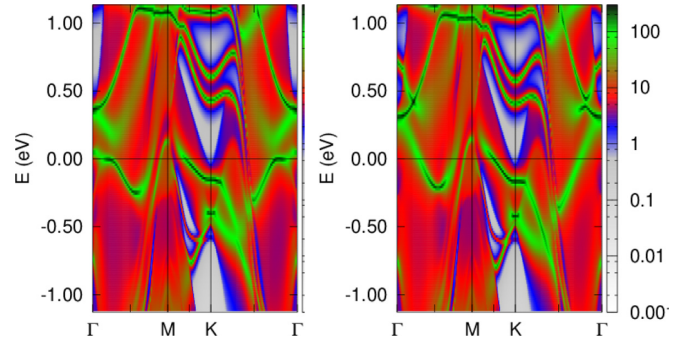


FIG. 10. Calculated Bloch spectral function $A(\mathcal{E}, \vec{k}, 0)$ (left) and $A(\mathcal{E}, \vec{k}, E)$, $E = -13.6 \frac{\text{V}}{\text{nm}}$ (right) representing the Fe-projected minority-spin states in 1 ML Fe on Pt(111).

such a behavior is not seen in the case of a “positive” electric field. From this one may conclude that the interface states are primarily responsible for the strong modification of the exchange parameters in the case of a “negative” electric field.

Due to the broken inversion symmetry at the surface, the Fe-Fe DMI does not vanish in the absence of the electric field in contrast to the unsupported Fe monolayer. As was mentioned above, the out-of-plane component of the DMI, D_{ij}^{out} , has an alternating orientation when going from one atom to another within the same neighbor shell, as is shown in Fig. 4. This results in a mutual cancellation of their influence on the magnetic structure. For that reason, we discuss here only the in-plane components of DMI D_{ij}^{in} , which are plotted in Fig. 8 (right panel) as a function of the field strength and direction. One can see a pronounced increase for the magnitude of the first- and third-neighbor parameters D_{01}^{in} and D_{03}^{in} in the case of a “negative” electric field. Note, however, that their sign is opposite. In the case of a “positive” electric field, the parameters D_{ij}^{in} have rather weak variation with the field strength. This behavior is rather similar to the behavior of the isotropic exchange interactions, and it can be related to the field-dependent changes of the interface electronic states.

To demonstrate the role of the substrate atoms for the DMI and its dependence on the electric field, additional calculations have been performed with an artificial scaling of the SOC on the Fe and the interface Pt atoms. When the SOC of the Fe atom is taken to be zero, $\text{SOC}(\text{Fe}) = 0$, the parameters D_{01}^{in} and D_{03}^{in} slightly increase, following the same field dependence as in the case of an unscaled SOC. In the case of D_{02}^{in} , the effect of $\text{SOC}(\text{Fe})$ scaling is much more pronounced, leading even to a change of sign for D_{02}^{in} . On the other hand, scaling SOC on the Pt atoms, $\text{SOC}(\text{Pt}) = 0$, leads to an increase of the magnitude of D_{02}^{in} (which is negative), having a rather similar field dependence as in the case of the unscaled SOC. These results obviously reflect a strong competition of the Pt and Fe SOC effects for the parameter D_{02}^{in} , with a leading effect of $\text{SOC}(\text{Fe})$. In contrast, in the case of $\text{SOC}(\text{Pt}) = 0$ the parameters D_{01}^{in} and D_{03}^{in} drop down significantly, which implies that their strength is governed by the SOC of the Pt atoms.

Finally, one should stress that in order to compare the calculated properties directly with experimental results, the structure parameters used in the calculations should be in

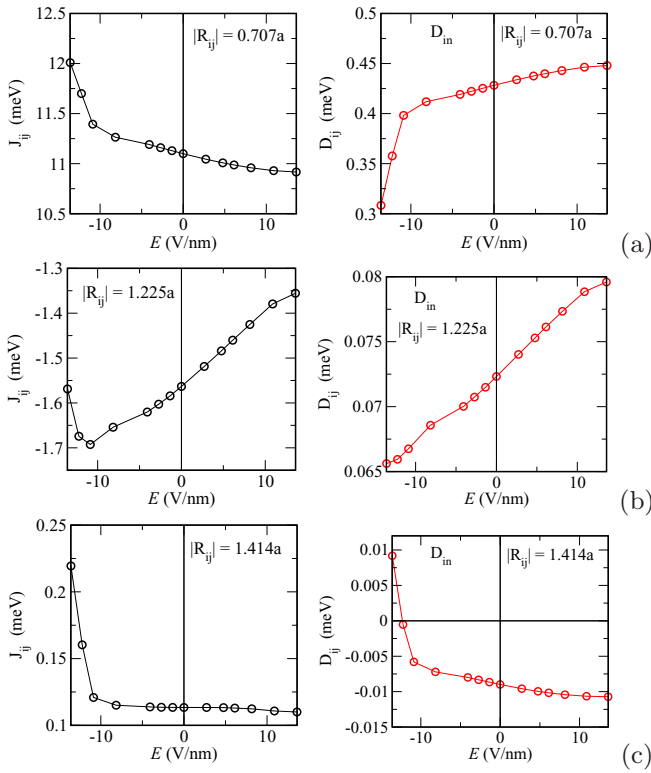


FIG. 11. 1 ML Fe on Pt(111) with 8% Fe-Pt interlayer relaxation: Isotropic Fe-Fe exchange-coupling parameter J_{ij} (left panel) and the maximal in-plane components of DMI, \bar{D}_{ij}^{in} (right panel), characterizing the interaction with the first neighbors at $R_{01} = 0.707a$ (a), the second neighbors at $R_{02} = 1.225a$ (b), and the third neighbors at $R_{03} = 1.414a$ (c), for 1 ML Fe on Pt(111). The parameters are plotted as a function of the applied electric field.

line with those of the real material. This concerns in particular the interlayer structure relaxation at the surfaces and interface in the case of layered systems, which should be taken into account in the calculations. To demonstrate its impact on the exchange parameters of the 1 ML Fe/Pt(111) system, the calculations have been performed using the Fe-Pt interlayer distance $d_{\text{Fe-Pt}}$ optimized by means of energy minimization, which led to a decrease of $d_{\text{Fe-Pt}}$ by about 8%. This relaxation results in a drastic change of the exchange parameters, even in the absence of an external electric field, as can be seen in Fig. 11. In particular, the nearest-neighbor isotropic exchange interaction is smaller by almost a factor of 2 when compared to the nonrelaxed system, while the DMI parameters increase by about the same ratio. Changes in this order of magnitude can be seen also for all other exchange parameters. As is to be expected, the modification of the electronic structure due to interlayer relaxation leads also to a modified field dependence of the exchange parameters J_{ij} and \bar{D}_{ij} that is shown in Fig. 11. In particular, in the nonrelaxed system strong changes have been observed for a negative electric field, while in the presence of relaxation comparable changes occur only at field strengths exceeding 10 V/nm. This behavior is attributed to the field-induced modification of the interface electronic structure in the vicinity of the Fermi level. To see whether these states survive in the relaxed sys-

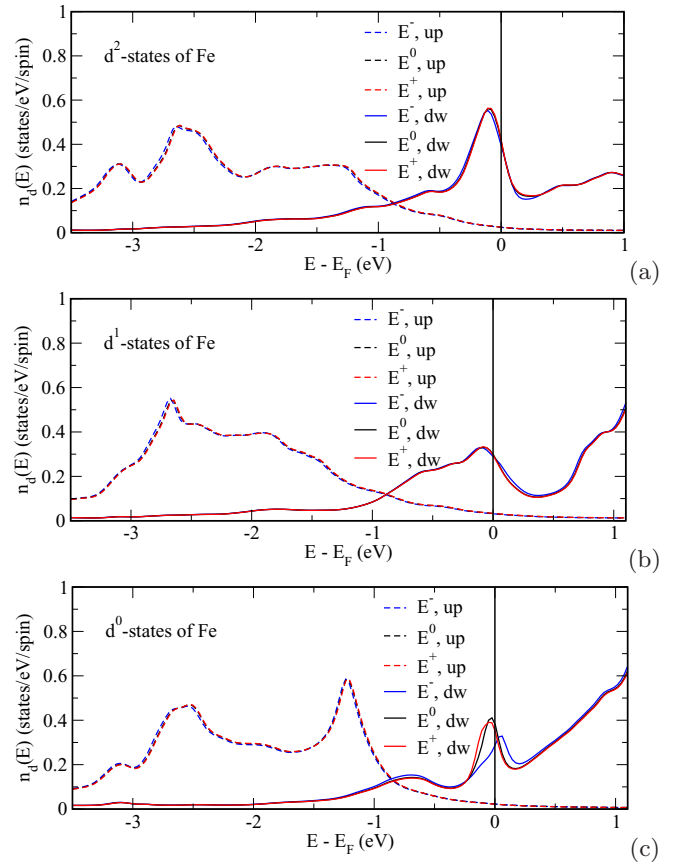


FIG. 12. Electric-field-induced change of the (l, m, s) -resolved density of states in the Fe layer on Pt(111). The applied electric field $E^0 = 0.0$ V/nm, $E^+ = +13.6$ V/nm, and $E^- = -13.6$ V/nm.

tem, we plot in Fig. 12 the (l, m, s) -resolved DOS calculated without, $E^+ = 0.0$ V/nm, and in the presence of an applied electric field, $E^+ = +13.6$ V/nm and $E^- = -13.6$ V/nm. The DOS for $d_{x^2-y^2}$, d_{xy} , d_{xz} , and d_{yz} states given in (a) and (b) shows a rather weak dependence on the electric field. A more pronounced modification is found only for the d_{z^2} states around the Fermi energy at $E^- = -13.6$ V/nm, although this modification is weaker when compared to the nonrelaxed system with the same applied electric field. We expect that these changes, similar to the case of the nonrelaxed system, are responsible for field-induced changes of the exchange parameters.

IV. 1 ML Fe on 1H-WS₂

In the case of 1 ML Fe on 1H-WS₂, the substrate was chosen as an example for an insulator in contrast to metallic Pt considered above. In this case, one can expect a different impact of the substrate on the Fe-Fe exchange interactions and in turn a different field-dependent behavior. The spin magnetic moment of Fe on 1H-WS₂ in the absence of an electric field is $2.72\mu_B$, which is essentially smaller when compared to $3.01\mu_B$ in the case of Fe/Pt(111), despite the larger Fe-Fe interatomic distance, 5.96 a.u. for 1H-WS₂, in comparison to 5.24 a.u. for Pt(111) as a substrate. Moving the Fe monolayer away from the surface of WS₂ by inserting an empty layer

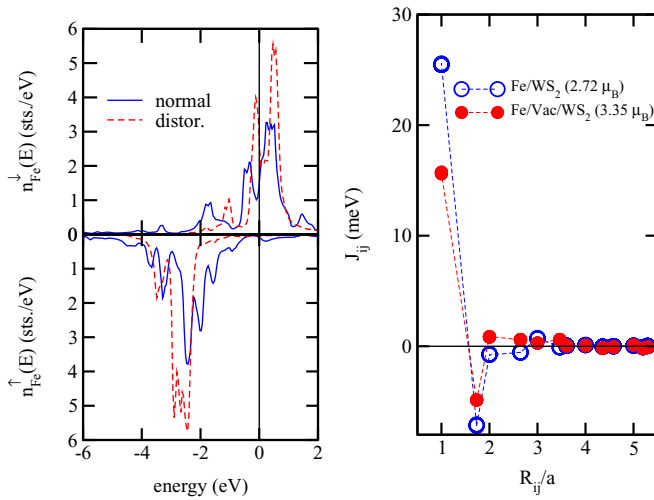


FIG. 13. Left panel: DOS for the nondistorted system (solid line) and for the distorted Fe/WS₂ system with empty monolayer inserted between Fe and substrate (dashed line). Right panel: isotropic Fe-Fe exchange parameters calculated for the nondistorted (open symbols) and distorted (full symbols) system.

in-between leads to an increase of the Fe spin magnetic moment to $3.35\mu_B$, which is a consequence of the narrower d -bands of Fe leading to more pronounced exchange splitting of the majority- and minority-spin states, as can be seen in the DOS for the Fe d -states plotted in Fig. 13 (left panel). This allows us to conclude that the decreased magnetic moment of Fe on 1H-WS₂ is a result of the strong hybridization of the Fe d states with the p states of S and d states of W.

The Fe-Fe exchange parameters calculated for the nondistorted Fe/WS₂ system (i.e., with identical Fe-S and W-S distances) are also plotted in Fig. 13 (right panel, open symbols) in comparison with those calculated for Fe monolayer spaced further away from the substrate (full symbols). From this one can see that depositing a Fe ML on WS₂ results in an increase of the exchange parameters despite the decrease of the spin magnetic moment of Fe. This trend is opposite to that found for 1 ML Fe/Pt(111) and may indicate a crucial role of the hybridization of the Fe d -states with the p -states of S responsible for a Fe-Fe superexchange in this system. As is shown in Fig. 14, the Fe magnetic moment m_{Fe} in Fe/1H-WS₂ has an almost linear dependence on the electric field. The field-induced change of m_{Fe} is larger by about an order of

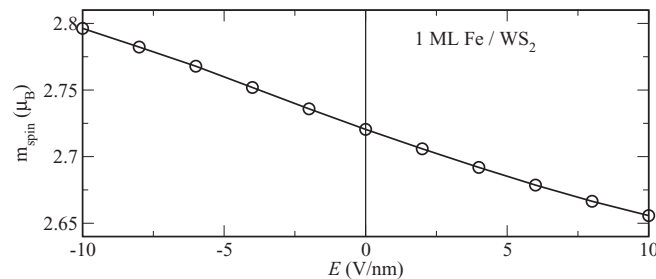


FIG. 14. Calculated spin magnetic moment of Fe, $m_{\text{Fe}}(E)$, as a function of the external electric field E for 1 ML Fe on 1H-WS₂.

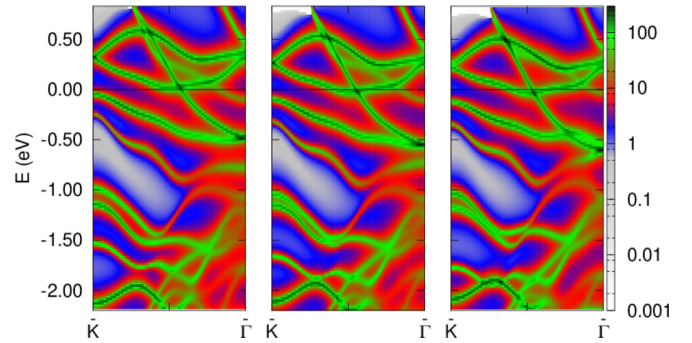


FIG. 15. Calculated Bloch spectral function $A(\mathcal{E}, \vec{k}, 0)$ (left), $A(\mathcal{E}, \vec{k}, E)$, $E = -10 \frac{\text{V}}{\text{nm}}$ (middle) and $A(\mathcal{E}, \vec{k}, E)$, $E = 10 \frac{\text{V}}{\text{nm}}$ (right) representing the states localized in Fe layer in 1 ML Fe on WS₂.

magnitude than in the case of Fe/Pt(111), as a result of the different impact of the substrate on Fe in these two cases.

Note also that in contrast to Fe/Pt(111), the whole Fe/1H-WS₂ system experiences the effect of the applied electric field due to its finite thickness. As a result, an impact of the electric field on the electronic structure is much stronger, as can be seen in the BSF $A(\mathcal{E}, \vec{k}, E)$ representing the Fe projected energy bands given in Fig. 15 for three different cases, $E = -10$, 0 , and $10 \frac{\text{V}}{\text{nm}}$.

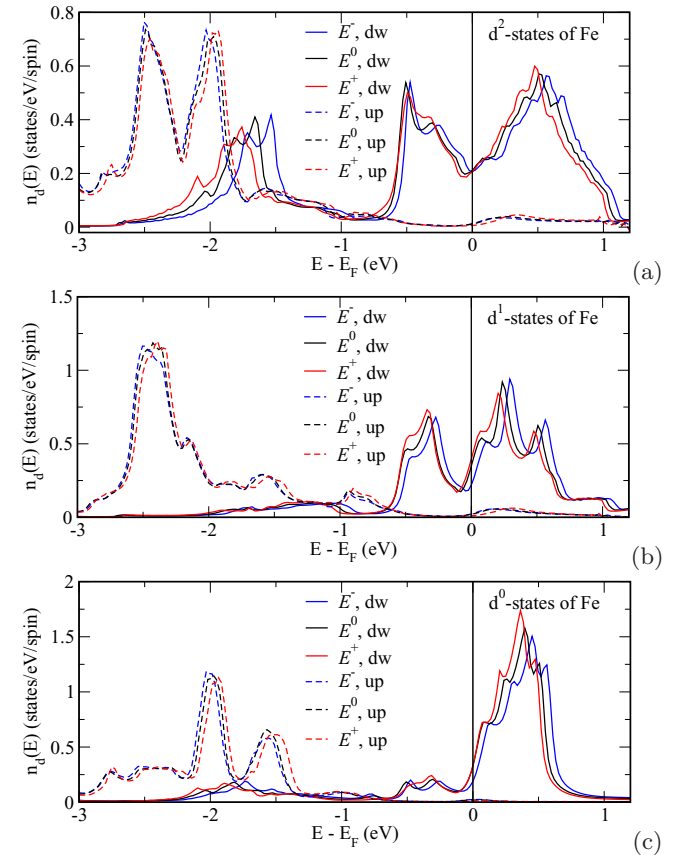


FIG. 16. Electric-field-induced change of the (l, m, s) resolved density of states in the Fe layer on top of WS₂. The applied electric field $E^0 = 0.0 \text{ V/nm}$, $E^+ = +10 \text{ V/nm}$ and $E^- = -10 \text{ V/nm}$. d^0 , d^1 , d^2 denote the d_{z^2} , (d_{xz}, d_{yz}) , and $(d_{xy}, d_{x^2-y^2})$ states, respectively.

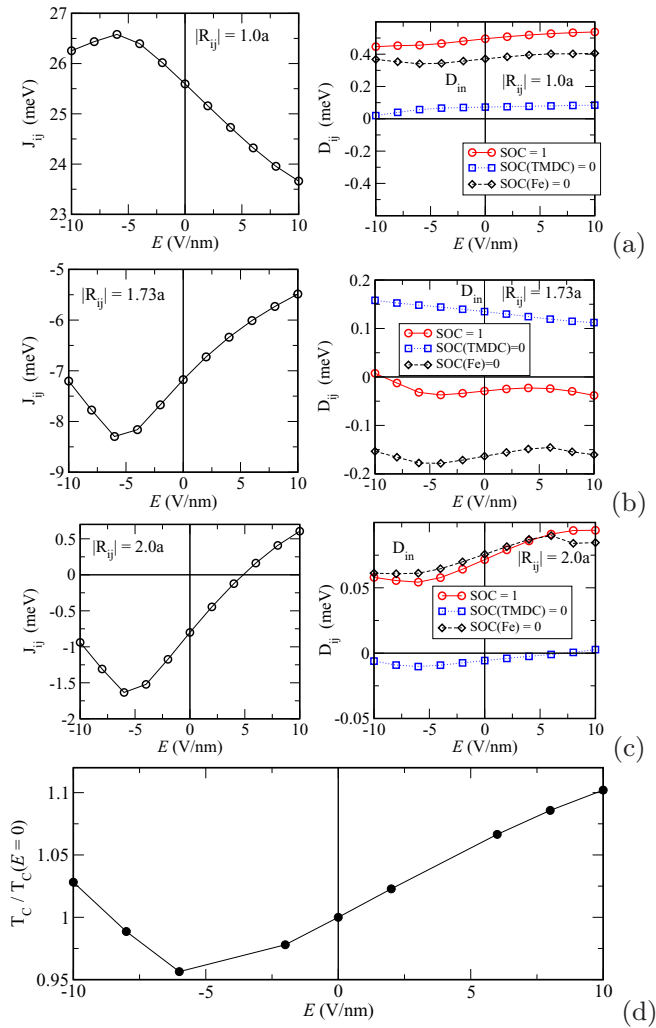


FIG. 17. Isotropic Fe-Fe exchange coupling parameter J_{ij} (left column) and in-plane (parallel to the surface plane) components of the Fe-Fe Dzyaloshinskii-Moriya interactions \bar{D}_{ij} (right column) with the first-neighbor, $R_{01} = a$ (a), second-neighbor, $R_{02} = 1.73a$ (b) and third-neighbor, $R_{03} = 2.0a$ (c), for 1 ML Fe on WS_2 . The parameters are presented as a function of the applied electric field. (d) the reduced mean-field Curie temperature $T_C/T_C(E=0)$, with $T_C(E=0) = 799$ K.

In the (l, m, s) -resolved DOS of Fe plotted in Fig. 16, one can see that the bandwidth of the d_{xy} and $d_{x^2-y^2}$ states is largest, indicating their strong hybridization with the states of the substrate, i.e., first of all p states of S. An applied electric field leads obviously to a rather complicated modification of the electronic structure. One notes a field-induced up- and down-shift of the minority-spin d -states of Fe arranged around the Fermi level, depending on the direction of the electric field [Figs. 16(a)–16(c)].

The DOS peaks at $E \approx -1.5$ eV in Fig. 16(a) appear due to a hybridization of the Fe minority-spin d_{xy} and $d_{x^2-y^2}$ states with the p -states of S and d -states of W. They show more pronounced field-induced shifts when compared to the states around the Fermi energy. This can be attributed to a field-induced change of the hybridization of these states caused by the shifts of the Fe d_{xy} and $d_{x^2-y^2}$ states. As a common trend,

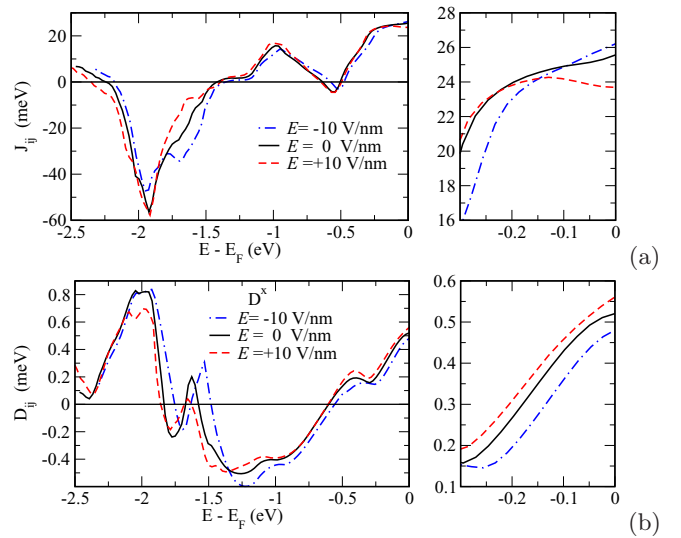


FIG. 18. Isotropic Fe-Fe exchange coupling parameter J^1 (a) and the in-plane $D^{1,\text{in}}$ (b) represented as a function of occupation of energy bands for 1 ML Fe on WS_2 . The applied electric field $E^0 = 0.0$ V/nm, $E^+ = +10$ V/nm, and $E^- = -10$ V/nm.

one notes for the majority-spin states a shift in the opposite direction in comparison with the minority-spin states, implying a field-induced change of the exchange splitting, leading in turn to a corresponding change of the spin magnetic moment of Fe.

The isotropic Fe-Fe exchange coupling parameters, J_{ij} , in 1 ML Fe on WS_2 are plotted in Fig. 17, left panel, as a function of applied electric field. Figures 17(a)–17(c) represent the exchange parameters for the distances $R_{01} = a$, $R_{02} = 1.73a$, and $R_{03} = 2.0a$, respectively. One can see in all cases an almost linear variation of J_{ij} for small electric fields. At larger fields, J_{ij} changes almost linearly with the field strength for the “positive” field, and it reaches some extremum in the case of the “negative” field. Figure 17(d) represents the reduced mean-field $T_C/T_C(E=0)$ evaluated assuming FM ordering in the system, demonstrating the rather pronounced impact of the electric field on the critical temperature.

The in-plane component Dzyaloshinskii-Moriya interactions in 1 ML Fe on WS_2 calculated for the distances $R_{01} = a$, $R_{02} = 1.73a$, and $R_{03} = 2.0a$ are plotted in Fig. 17, right panel, as a function of applied electric field. In contrast to the Fe/Pt(111) system, the DMI exhibits a weaker dependence on the electric field, implying a crucial role of the states localized at the Fe/substrate interface, being rather sensitive to the influence of an electric field. Such states occur in the vicinity of the Fermi energy for the Fe/Pt(111) interface, but not for the Fe/ WS_2 system. A strong field-induced modification of the Fe d -states in Fe/ WS_2 occurs due to a change of their hybridization with the electronic states of substrate. This, however, corresponds mainly to the states below the Fermi energy. As one can see in Fig. 18(b) representing the in-plane DMI as a function of the occupation of the electronic states, the field-induced change of the hybridization could result in a much stronger field dependence of DMI in the case of the Fermi level shifted down by about 1.5 eV.

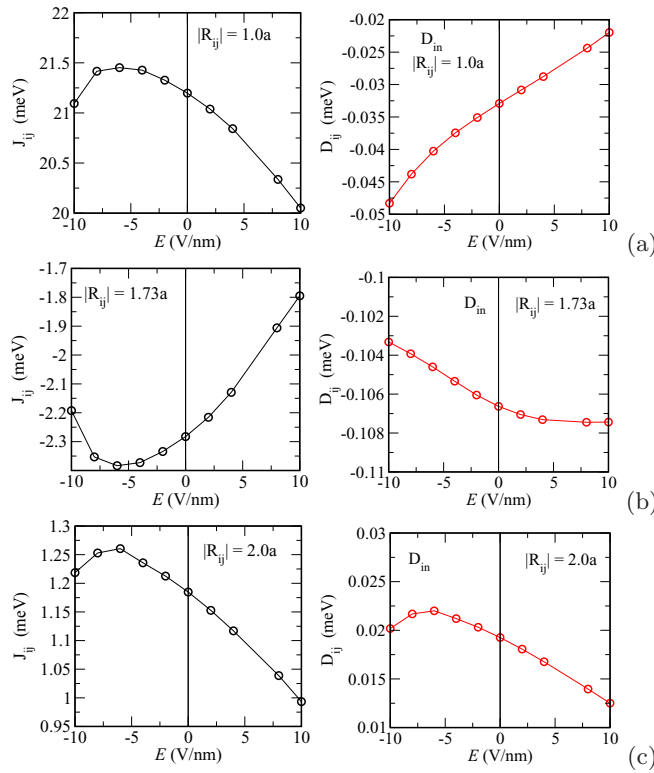


FIG. 19. Isotropic Fe-Fe exchange parameter J_{ij} (left column) and in-plane (parallel to the surface plane) components of the Fe-Fe Dzyaloshinskii-Moriya interactions \vec{D}_{ij} (right column) with the first neighbor, $R_{01} = a$ (a), second neighbor, $R_{02} = 1.73a$ (b), and third neighbor, $R_{03} = 2.0a$ (c), for 1 ML Fe on WS_2 with the Fe-S interlayer distance decreased by 8%. The parameters are presented as a function of the applied electric field.

Note that according to the results shown in Fig. 17, the SOC of the substrate plays a leading role for the \vec{D}_{01} and \vec{D}_{03} parameters, similar to the case of Fe/Pt(111), while for \vec{D}_{03} the SOC for Fe and the WS_2 substrate compete with each other.

As a crucial role of the interlayer relaxation for the exchange parameters was demonstrated above for 1 ML Fe/Pt(111), one can expect significant changes of these parameters also for a Fe monolayer deposited on WS_2 . For that reason, the calculations have been performed for the Fe/ WS_2 system with the Fe-S interlayer distance decreased by 8%,

i.e., taking the same interlayer modification as in the case of Fe/Pt(111). The dependence of the exchange parameters on the applied electric field for such a system is plotted in Fig. 19. When comparing with Fig. 17, first of all, one can see substantial changes for the J_{ij} and \vec{D}_{ij} parameters obtained for the field-free system, although these changes are not so pronounced as in the case of Fe/Pt(111). The first- and second-neighbor isotropic parameters decrease in magnitude, while the third-neighbor parameter even changes sign. In contrast to Fe/Pt(111), the first-neighbor DMI parameter also strongly decreases when compared to the nonrelaxed system. Considering the field-dependent changes of the exchange parameters, one can see that the behavior of the first- and second-neighbor isotropic exchange and DMI parameters is similar to that obtained for the nonrelaxed system. This is in contrast to Fe/Pt(111), for which rather strong changes of the field-dependent behavior occurs for almost all exchange parameters.

It should be noted that in order to make a comparison with experiment, more detailed investigations on the structural relaxation in 1 ML Fe on WS_2 , involving the relaxation of the volume as well as of the W-S distances, are needed. This, however, goes well beyond the scope of the present work and deserves a separate investigation.

V. SUMMARY

In summary, considering an Fe monolayer, free-standing and deposited on two different substrates, we demonstrated the impact of an applied electric field on the exchange parameters, both isotropic J_{ij} and DMI \vec{D}_{ij} . In the case of the free-standing Fe monolayer, the electric field has a key role creating the DMI by breaking the inversion symmetry in the system. In the case of deposited Fe films, rather prominent changes of the exchange parameters occur for the Fe/Pt(111) system due to the localized electronic states at the Fe/Pt interface, which are strongly affected by the electric field. In the case of a TMDC substrate, the dependence of DMI on the electric field is much weaker, although the isotropic interactions still exhibit a rather strong modification.

ACKNOWLEDGMENT

This work was supported by Deutsche Forschungsgemeinschaft Grant No. DFG EB 154/35.

- [1] K. Siratori and E. Kita, *J. Phys. Soc. Jpn.* **48**, 1443 (1980).
- [2] T. Jungwirth, J. Sinova, J. Mašek, J. Kučera, and A. H. MacDonald, *Rev. Mod. Phys.* **78**, 809 (2006).
- [3] F. Matsukura, Y. Tokura, and H. Ohno, *Nat. Nanotechnol.* **10**, 209 (2015).
- [4] H. Katsura, A. V. Balatsky, and N. Nagaosa, *Phys. Rev. Lett.* **98**, 027203 (2007).
- [5] T. Maruyama, Y. Shiota, T. Nozaki, K. Ohta, N. Toda, M. Mizuguchi, A. A. Tulapurkar, T. Shinjo, M. Shiraishi, S. Mizukami, Y. Ando, and Y. Suzuki, *Nat. Nanotechnol.* **4**, 158 (2009).
- [6] M. Ishibashi, K. T. Yamada, Y. Shiota, F. Ando, T. Koyama, H. Kakizakai, H. Mizuno, K. Miwa, S. Ono, T. Moriyama, D. Chiba, and T. Ono, *Appl. Phys. Express* **11**, 063002 (2018).
- [7] T. Nozaki, Y. Shiota, S. Miwa, S. Murakami, F. Bonell, S. Ishibashi, H. Kubota, K. Yakushiji, T. Saruya, A. Fukushima, S. Yuasa, T. Shinjo, and Y. Suzuki, *Nat. Phys.* **8**, 491 (2012).
- [8] C.-G. Duan, J. P. Velev, R. F. Sabirianov, Z. Zhu, J. Chu, S. S. Jaswal, and E. Y. Tsymlal, *Phys. Rev. Lett.* **101**, 137201 (2008).
- [9] G. T. Rado, *Phys. Rev. Lett.* **6**, 609 (1961).
- [10] K. T. Yamada, M. Suzuki, A.-M. Pradipto, T. Koyama, S. Kim, K.-J. Kim, S. Ono, T. Taniguchi, H. Mizuno, F. Ando, K. Oda,

- H. Kakizakai, T. Moriyama, K. Nakamura, D. Chiba, and T. Ono, *Phys. Rev. Lett.* **120**, 157203 (2018).
- [11] Y. Yamada, K. Ueno, T. Fukumura, H. T. Yuan, H. Shimotani, Y. Iwasa, L. Gu, S. Tsukimoto, Y. Ikuhara, and M. Kawasaki, *Science* **332**, 1065 (2011).
- [12] A. Obinata, Y. Hibino, D. Hayakawa, T. Koyama, K. Miwa, S. Ono, and D. Chiba, *Sci. Rep.* **5**, 14303 (2015).
- [13] K. Nakamura, R. Shimabukuro, Y. Fujiwara, T. Akiyama, T. Ito, and A. J. Freeman, *Phys. Rev. Lett.* **102**, 187201 (2009).
- [14] M. Weisheit, S. Fähler, A. Marty, Y. Souche, C. Poinignon, and D. Givord, *Science* **315**, 349 (2007).
- [15] D. Lebeugle, A. Mougín, M. Viret, D. Colson, and L. Ranno, *Phys. Rev. Lett.* **103**, 257601 (2009).
- [16] D. Chiba, Y. Nakatani, F. Matsukura, and H. Ohno, *Appl. Phys. Lett.* **96**, 192506 (2010).
- [17] M. Date, J. Kanamori, and M. Tachiki, *J. Phys. Soc. Jpn.* **16**, 2589 (1961).
- [18] G. T. Rado and V. J. Folen, *J. Appl. Phys.* **33**, 1126 (1962).
- [19] V. Laukhin, V. Skumryev, X. Martí, D. Hrabovský, F. Sánchez, M. V. García-Cuenca, C. Ferrater, M. Varela, U. Lüders, J. F. Bobo, and J. Fontcuberta, *Phys. Rev. Lett.* **97**, 227201 (2006).
- [20] H. Katsura, N. Nagaosa, and A. V. Balatsky, *Phys. Rev. Lett.* **95**, 057205 (2005).
- [21] H. Ohno, D. Chiba, F. Matsukura, T. Omiya, E. Abe, T. Dietl, Y. Ohno, and K. Ohtani, *Nature (London)* **408**, 944 (2000).
- [22] D. Chiba, M. Yamanouchi, F. Matsukura, and H. Ohno, *Science* **301**, 943 (2003).
- [23] I. V. Ovchinnikov and K. L. Wang, *Phys. Rev. B* **79**, 020402(R) (2009).
- [24] K. Shimamura, D. Chiba, S. Ono, S. Fukami, N. Ishiwata, M. Kawaguchi, K. Kobayashi, and T. Ono, *Appl. Phys. Lett.* **100**, 122402 (2012).
- [25] F. Ando, K. T. Yamada, T. Koyama, M. Ishibashi, Y. Shiota, T. Moriyama, D. Chiba, and T. Ono, *Appl. Phys. Express* **11**, 073002 (2018).
- [26] M. Oba, K. Nakamura, T. Akiyama, T. Ito, M. Weinert, and A. J. Freeman, *Phys. Rev. Lett.* **114**, 107202 (2015).
- [27] T. Srivastava, M. Schott, R. Juge, V. Křížáková, M. Belmeguenai, Y. Roussigné, A. Bernand-Mantel, L. Ranno, S. Pizzini, S.-M. Chérif, A. Stashkevich, S. Auffret, O. Boulle, G. Gaudin, M. Chshiev, C. Baraduc, and H. Béa, *Nano Lett.* **18**, 4871 (2018).
- [28] W. Zhang, H. Zhong, R. Zang, Y. Zhang, S. Yu, G. Han, G. L. Liu, S. S. Yan, S. Kang, and L. M. Mei, *Appl. Phys. Lett.* **113**, 122406 (2018).
- [29] F. Ando, H. Kakizakai, T. Koyama, K. Yamada, M. Kawaguchi, S. Kim, K.-J. Kim, T. Moriyama, D. Chiba, and T. Ono, *Appl. Phys. Lett.* **109**, 022401 (2016).
- [30] M. Schott, L. Ranno, H. Bea, C. Baraduc, S. Auffret, and A. Bernand-Mantel, *J. Magn. Magn. Mater.* **520**, 167122 (2021).
- [31] T. Koyama, Y. Nakatani, J. Ieda, and D. Chiba, *Sci. Adv.* **4**, eaav0265 (2018).
- [32] H. Yang, O. Boulle, V. Cros, A. Fert, and M. Chshiev, *Sci. Rep.* **8**, 12356 (2018).
- [33] S. Paul and S. Heinze, [arXiv:2104.11986](https://arxiv.org/abs/2104.11986), (2021).
- [34] H. Ebert *et al.*, The Munich SPR-KKR package, version 8.6, <https://www.ebert.cup.uni-muenchen.de/en/software-en/13-sprkkkr> (2021).
- [35] H. Ebert, D. Ködderitzsch, and J. Minár, *Rep. Prog. Phys.* **74**, 096501 (2011).
- [36] S. H. Vosko, L. Wilk, and M. Nusair, *Can. J. Phys.* **58**, 1200 (1980).
- [37] E. Simon, A. Marmodoro, S. Mankovsky, and H. Ebert, *Phys. Rev. B* **103**, 064406 (2021).
- [38] N. D. Mermin and H. Wagner, *Phys. Rev. Lett.* **17**, 1133 (1966).
- [39] P. Bruno, *Phys. Rev. B* **43**, 6015 (1991).
- [40] I. Turek, J. Kudrnovský, V. Drchal, and P. Bruno, *Philos. Mag.* **86**, 1713 (2006).
- [41] Y. A. Bychkov and E. I. Rashba, *Zh. Eksp. Teor. Fiz.* **39**, 66 (1984) [*Sov. J. Exp. Theo. Phys. Lett.* **39**, 78 (1984)].
- [42] A. Kundu and S. Zhang, *Phys. Rev. B* **92**, 094434 (2015).